Published in final edited form as:
Toxicol Appl Pharmacol. 2009 May 15; 237(1): 29–40. doi:10.1016/j.taap.2008.06.025.

Uncoupling nicotine mediated motoneuron axonal pathfinding errors and muscle degeneration in zebrafish

Lillian Welsh[a], **Robert L. Tanguay**[b], and **Kurt R. Svoboda**[a,*]

[a]Department of Biological Sciences, Louisiana State University, Baton Rouge, Louisiana, 70803, USA

[b]Department of Environmental and Molecular Toxicology, Oregon State University, Corvallis Oregon, 97331, USA

Abstract

Zebrafish embryos offer a unique opportunity to investigate the mechanisms by which nicotine exposure impacts early vertebrate development. Embryos exposed to nicotine become functionally paralyzed by 42 hpf suggesting that the neuromuscular system is compromised in exposed embryos. We previously demonstrated that secondary spinal motoneurons in nicotine-exposed embryos were delayed in development and that their axons made pathfinding errors (Svoboda, K.R., Vijayaraghaven, S., Tanguay, R.L., 2002. Nicotinic receptors mediate changes in spinal motoneuron development and axonal pathfinding in embryonic zebrafish exposed to nicotine. J. Neurosci. 22, 10731–10741). In that study, we did not consider the potential role that altered skeletal muscle development caused by nicotine exposure could play in contributing to the errors in spinal motoneuron axon pathfinding. In this study, we show that an alteration in skeletal muscle development occurs in tandem with alterations in spinal motoneuron development upon exposure to nicotine. The alteration in the muscle involves the binding of nicotine to the muscle-specific AChRs. The nicotine-induced alteration in muscle development does not occur in the zebrafish mutant (*sofa potato*, [*sop*]), which lacks muscle-specific AChRs. Even though muscle development is unaffected by nicotine exposure in *sop* mutants, motoneuron axonal pathfinding errors still occur in these mutants, indicating a direct effect of nicotine exposure on nervous system development.

Keywords

Motoneuron; Axonal pathfinding; Muscle degeneration; Sofa potato

Introduction

In zebrafish, as in other vertebrates, the axial musculature is made up of three types of fibers: slow (red) fibers, fast (white) fibers, and intermediate fibers (van Raamsdonk et al., 1978; Sherwood, 1995; te Kronnie, 2000). The slow fibers are equipped for oxidative phosphorylation, can generate relatively large stores of energy, and are most resistant to fatigue. The fast fibers are least resistant to fatigue because they rely on anaerobic glycolysis for ATP generation. Intermediate fibers share both of these characteristics. They contract more rapidly than slow fibers, but can remain contracted longer than fast fibers (Sherwood, 1995). In

*Corresponding author. Fax: +1 225 578 2597. ksvobo1@lsu.edu(K.R. Svoboda).

Appendix A. Supplementary data

Supplementary data associated with this article can be found, in the online version, at doi:10.1016/j.taap.2008.06.025.

zebrafish, slow muscle fibers are derived from adaxial cells that develop laterally from the periphery of the notochord (Devoto et al., 1996). A subset of adaxial cells delineate what is known as the common path, where all motoneuron axons initially migrate before projecting to their respective targets. These adaxial cells release signals that guide motoneuron axon pathfinding (Zeller and Granato, 1999; Zeller et al., 2002). As the first motoneuron growth cones enter the common pathway, the adaxial cells migrate laterally and ultimately give rise to the slow muscle found at the lateral surface of the somites (Devoto et al., 1996).

It is well-established that vertebrate muscle development and its activity are tightly coupled to motoneuron development. In developing chick, blockade of neuromuscular activity causes hyperbranching of motoneuron axons (Pittman and Oppenheim, 1979; Dahm and Landmesser, 1988; Landmesser, 1992). The zebrafish mutant *twister* (*chrna1*$^{dtbn12/dtbn12}$ referred to as *twi* from here onward) has increased neuromuscular activity during motoneuron development (Lefebvre et al., 2004). At the physiological level, the muscle-specific AChR in *twi* skeletal muscle is overactive as revealed by longer decay times for acetylcholine evoked endplate currents. In homozygous *twi* mutants, primary motoneuron axons can be either stalled in development or exhibit ectopic branches. Both slow and fast skeletal muscle in homozygous *twi* embryos appear degenerated. In heterozygous *twi* embryos, the motoneuron phenotype is reduced in severity, but *still* persists. Thus, prolonged neuromuscular activity (heterozygous or homozygous *twi*) or severe muscle degeneration (homozygous *twi*) can influence motoneuron development.

In other zebrafish paradigms, when muscle development is compromised, motoneuron axonal pathfinding errors often occur. In mutants that have been identified in genetic screens, abnormal muscle development or somite formation often, but not always, occur in parallel with abnormal motoneuron development (Birely et al., 2005; van Eeden et al., 1996). In toxological studies, when zebrafish embryos are exposed to cadmium, both muscle development and primary motoneuron development are altered (Chow and Cheng, 2003). Thus, it is often unclear whether a toxicant such as cadmium alters motoneuron development directly, or if it indirectly alters motoneuron development by altering muscle development.

In our previous study (Svoboda et al., 2002), we demonstrated that nicotine exposure altered zebrafish embryonic motoneuron development. Nicotine could also potentially degenerate muscle fibers by over-stimulation of skeletal muscle-specific AChRs. This over-stimulation itself could contribute to errors in motoneuron axonal pathfinding, or it could result in muscle degeneration which could in turn influence motoneuron axonal pathfinding. In this paper, we demonstrate that nicotine exposure during embryonic development results in abnormal slow and fast muscle morphology. We also demonstrate that nicotine exposure does not alter slow and fast muscle development in the paralytic mutant zebrafish chrnd$^{tj19d/tj19d}$, formerly known as *sofa potato*, which lacks skeletal muscle-specific AChRs (Ono et al., 2001).

Using chrnd$^{tj19d/tj19d}$ mutants, it was found that axonal pathfinding errors caused by embryonic nicotine exposure can occur independently of any confounding, nicotine-induced abnormal muscle phenotypes. Collectively, these results indicate that nicotine exposure directly affects CNS development independently of nicotine-induced muscle degeneration or over-activity.

Materials and methods

Zebrafish embryos and chemical exposure

Fertilized eggs were obtained from natural spawnings of adult zebrafish according to the *Zebrafish Book* (Westerfield, 1995). Adult fish were maintained at 28.2 °C with a lighting schedule of 14 h light and 10 h dark. Embryos were collected within 3 h of spawning, rinsed, placed into 10 cm petri dishes and raised until 21–22 h post-fertilization (hpf). In this study,

embryos from wild-type, *Tg(isl1:GFP)*, referred to as *isl1* hereafter, and identified heterozygous parents which have a point mutation in the chrnd subunit of the zebrafish muscle acetylcholine receptor were used. This mutant line of fish chrnd^{tj19d} is known as the *sofa potato* mutant and will be referred to as *sop* hereafter. We use the nomenclature *sop*$^{+/?}$ to describe *sop* sibling embryos. When crossing two heterozygote carriers for the *sop* mutation, the prodigy would be 25% $^{+/+}$, 25% $^{-/-}$ and 50% heterozygous $^{+/-}$. However, we have no way to distinguish between the $^{+/+}$ embryos or $^{+/-}$ embryos and refer to these siblings collectively as *sop*$^{+/?}$.

The wild-type embryos used in this study were obtained from the AB, WIK, and TL strains of zebrafish as well as fishery-reared adults obtained from Ekwill Waterlife Resources (Gibsonton, FL). The effects presented in this study were not dependent on the fish strain used.

At 21–22 hpf, embryos were exposed to embryo medium containing nicotine (15 or 30 μM), epibatidine (125 nM–1 μM) or tricaine (0.006%–0.01%), and then raised until 72 hpf. All exposures were performed in 5 cm diameter petri dishes containing 5 ml of embryo medium with the various reagents. Experiments were replicated with a minimum of 10 embryos per exposure. In experiments using *sop*$^{-/-}$ embryos, a minimum of 5 embryos were exposed. At the end of the exposures, larvae were prepared for anatomical analysis.

The (−)-nicotine used in this study was purchased from Sigma (St. Louis, Missouri, USA, catalog # N3876-5ml). Nicotine stock solutions were made in distilled water and then diluted in embryo medium to obtain final concentrations. Fresh nicotine was made daily as needed for all experiments. Epibatidine was purchased from Tocris Bioscience (Ellisville, MO, USA) and was diluted in distilled water to a stock solution. It was then diluted in embryo medium to obtain final experimental concentrations ranging between 125 nM and 1 μM. Tricaine (MS222) was purchased from Sigma and made per instructions in the Zebrafish Book (Westerfield, 1995).

Behavior

To determine if nicotine had successfully penetrated the embryos, a touch response was initiated by applying a tactile stimulus to the tail region of 48 hpf embryos. This touch response is a motor behavior that occurs in response to a tactile stimulus and serves to move the fish in a direction away from the stimulus. At 48–72 hpf, embryos exposed to 30 μM nicotine lack a touch response (Svoboda et al., 2002). Using this behavioral criterion, we were able to establish that the nicotine was penetrating the embryo at this concentration.

Live imaging in transgenic isl1 larvae

Images of live *isl1* larvae were acquired using a ORCA-ER digital camera (Hamamatsu Photonics) mounted to a Zeiss Axiovert 200M inverted microscope using a 20× dry objective and equipped with epi-fluorescence. For each experiment, we determined the exposure setting required to get a non-saturating image of axonal GFP expression in control larvae. For any particular experiment, the control images were acquired first and images of the larvae exposed to nicotine were acquired using the same exposure times as controls. In some instances, the exposure settings saturated the somatic GFP expression, thus those images were cropped for presentation purposes. Animal protocols were approved by the Institutional Animal Care and Use Committee at Louisiana State University.

Morphological techniques

Whole-mount immunohistochemistry was carried out using a modified version from previous published protocols (Svoboda et al., 2001, 2002, Pineda et al., 2006). Larvae processed for immunohistochemistry were first fixed in 4% paraformaldehyde overnight at 2–4 °C and then

stored in PBS. After permeablization, they were incubated in a primary antibody overnight at 2–4 °C. Primary antibodies were used at the following dilutions: F59: 1:50; F310: 1:250; znp1: 1:250; zn5: 1:500; anti-β2 nAChR: 1:500. These primary antibodies were used to label slow muscle fibers (F59), fast muscle fibers (F310), primary motoneuron axons (znp1), secondary motoneuron axons (zn5) and the nAChR β2 subunit (anti-β2 nAChR). Monoclonal antibodies (F59, F310 and znp1) were purchased from the Developmental Studies Hybridoma Bank, The University of Iowa, Iowa City, Iowa. Zn5 was originally obtained from the University of Oregon Zebrafish International Research Center. It is no longer in production, but zn8, which is a duplicate isolate of the same hybridoma as zn5 (Kawahara et al., 2002), is available from the Developmental Studies Hybridoma Bank and the Zebrafish International Research Center at the University of Oregon. The polyclonal anti-β2 nAChR was made by Antibodies, Inc., Davis California.

The following day, the samples were washed for 60 min in PBST and then incubated in a fluorescent secondary antibody, Alexa 488 or 546 (1:1000–2000 dilution) for 90 min. They were then rinsed in PBST for another 60 min and prepared for image analysis.

Visualization of antibody staining

Samples that had been processed for znp1, zn5, F59, F310, or anti-β2 nAChR immunoreactivity were mounted laterally, viewed on a Zeiss Axiovert 200 M inverted microscope equipped with a Zeiss ApoTome while using a 20× (dry) or 40× (oil) objective (0.40 and 1.3 numerical apertures respectively), and photographed using an ORCA-ER digital camera. In some instances, *z*-series (stacks) were acquired with the ApoTome inserted into the light path of the microscope. As was the case for the imaging of live embryos, exposure times were constant for control and treated embryos. All acquired images were digitally processed with the aid of Adobe Photoshop 7.0 (Adobe Systems, San Jose, CA). For each image of a whole-mount larvae, the head (anterior) is to the left and dorsal is at the top. We focused our image acquisition on the region of spinal cord and associated musculature over the yolk sac extension. This is the same region of interest from where the muscle cross-sections described below were obtained.

Muscle histology

Larvae were fixed overnight at 2–4 °C in 4% paraformaldehyde, and then rinsed overnight in PBS with 0.1% Tween. The PBS was removed and completely replaced with distilled water. A dehydration series starting with 50% ethanol followed in which, over the course of 2 h, ethanol was gradually added to the water until 95% ethanol was achieved. The solution was then entirely replaced with 95% ethanol and then with 100% ethanol. The embryos were then infiltrated overnight at 28 °C in a 1:1 solution of 100% ethanol and LR White resin (a 1:1 combination of hard and medium grade). The solution was then replaced with only the combination grade resin for 4 h after which the embryos were embedded in the resin overnight at 62 °C. 500 nm cross-sections were cut from the region above the center of the yolk sac extension with a DuPont 5000 ultra microtome, mounted on glass slides, stained with toluidine blue, and imaged.

Gross morphology— cross-sections

Images of cross-sections were obtained using an RTSpot digital camera (Roper Scientific, Trenton, NJ) mounted to a Nikon (Tokyo, Japan) upright microscope with a 20× (dry) or 40× (dry) objective. Morphological analysis of each larva was performed using the software package Image-Pro Plus 4 (Media Cybernetics, Silver Spring, MD). Images randomly chosen from each individual larva were magnified to allow for easy visualization of each cross-section of tissue. For each cross-section obtained from control and experimental larvae, a straight line was drawn from the dorsal most extent of the muscle mass to the dorsal side of the gut region.

The lengths of each of these lines were measured in pixels and converted *post hoc* to provide lengths in micrometers.

Slow muscle morphology— whole mounts

From individual experiments, images of F59-stained control and experimental embryos were randomly chosen and analyzed with Image-Pro Plus 4. For each fiber measured, we arbitrarily measured the fiber width at the center of a given segment of muscle.

Generation of zebrafish nAChR β2 antibody and morpholino

To generate zebrafish-specific anti-nAChR β2 polyclonal antibodies, the human nAChR β2 nucleotide sequence was queried in GenBank to identify the zebrafish nAChR β2 ortholog (accession number XM_001343008). ClustalW2 was used to align the known human and zebrafish nAChR and a β2 subtype specific peptide (RSNVRERFRRKHQRKSFSC) was designed which spanned positions 336–353 of the zebrafish protein. The KLH-conjugated peptide specific antibody was developed in rabbits by Antibodies Inc, (Davis, CA). Control and nAChR β2-targeting morpholinos (MO)were generated by GeneTools (Philomath, OR). The standard control MO (5′CTCTTACCTCAGTTACAATTTATA3′) was used as an injection control and the translation start site blocking nAChR β2 oligo (5′ GAAAATCTTTAAACCACTTCGCCAT 3′) was used to repress nAChR β2 translation. For all morpholinos studies, MO were diluted to 3 mM in 1 × Danieau's solution (58 mM NaCl, 0.7 mM KCl, 0.4 mM MgSO4, 0.6 mM Ca(NO3)2, 5 mM HEPES, pH 7.6). Approximately 2 nl of 0.3 mM of the MO solution was microinjected into the embryos at the 1–2 cell stage.

Statistics

All results are presented as means ± SE. Significant differences between means were determined using a Student's *T*-Test with significance being indicated by p values of <0.05.

Results

Axonal pathfinding errors coincide with muscle degeneration in nicotine-exposed embryos

In our previous study characterizing motoneuron development in nicotine-exposed embryos (Svoboda et al., 2002), we noticed that the embryos became paralyzed, likely indicating a nicotine interaction with muscle acetylcholine receptors. The primary focus of that study was secondary motoneuron development, and did not address the consequences of nicotine exposure to the muscle. In the present study, secondary motoneuron but not primary motoneuron development, was analyzed in the context of potential nicotine-induced muscle phenotypes.

Embryos exposed to nicotine were smaller in the dorsal/ventral axis compared to unexposed embryos (Figs. 1A, C), a result consistent with our previous findings (Svoboda et al., 2002). When cross-sections from the trunk musculature were analyzed, we detected disorganized atrophic muscle (Fig. 1B). At the cross-section level, the white fast muscle fibers comprise the bulk of the muscle mass, whereas the red slow muscle fibers can sometimes be detected at the periphery (Fig. 1B, left). Both slow muscle and fast muscle were altered by nicotine exposure (30 μM exposure is presented in Fig. 1B, right). This finding was evident in all the wild-type lines analyzed as well as the transgenic *isl1* line. Embryos of the *isl1* line express GFP in secondary motoneurons (Svoboda et al., 2002; Higashijima et al., 2000) and are also sensitive to nicotine exposure.

We then attempted to determine if motoneuron axonal pathfinding errors coincided with the nicotine-induced muscle degeneration. *Isl1* zebrafish embryos (22 hpf) were exposed to nicotine until 72 hpf. In living *isl1* embryos exposed to 15–30 μM nicotine, axons of secondary

motoneurons had problems in pathfinding (Fig. 2A). Those same individual fish were then analyzed by light microscopy to evaluate muscle fiber organization. In larvae that exhibited axonal pathfinding errors resulting from nicotine exposure, the muscle was disorganized and the fibers appeared smaller and sometimes degenerated compared to muscle fibers from non-exposed larvae (Figs. 2B, C).

It was sometimes difficult to determine if the peripheral slow muscle had degenerated in the exposed larvae or if what we were observing was actually degenerated white muscle fibers. To circumvent this problem, whole-mount immunohistochemistry using the monoclonal F59 antibody was performed to reveal slow muscle fibers in *isl1* nicotine-exposed larvae. In some experiments, living larvae were imaged prior to being processed for immunohistochemistry. In the *isl1* nicotine-exposed larvae that exhibited axonal pathfinding errors (Fig. 3A), slow muscle fibers were thinner compared to slow muscle fibers in non-exposed larvae (Fig. 3B). Thus, nicotine exposure caused both a motoneuron phenotype and a muscle phenotype in *isl1* zebrafish embryos. Once this was established, we characterized the muscle morphology in non-transgenic, wild-type embryos exposed to nicotine to ensure that the nicotine-induced muscle phenotypes were robust and reproducible regardless of the genetic background of the embryo.

Sofa potato paralytic zebrafish

To determine whether the muscle defects or the over-activation of muscle AChRs by nicotine exposure influenced the motoneuron phenotypes, we performed experiments in *sop* zebrafish mutants. $Sop^{-/-}$ larvae lack skeletal muscle acetylcholine receptors and are consequently paralyzed (Ono et al. 2001). Even though these larvae lack skeletal muscle AChRs, we found their muscle and motoneuron development to be quite normal. However, when cross-sections were analyzed, $sop^{-/-}$ larvae were smaller along the dorsal/ventral axis compared to stage matched siblings or stage matched wild-types (see Fig. 6C for actual numbers, compare vertical reference bars in Fig. 1A wild-type and Fig. 4B). This phenotype may be related to the inability of the embryos to move. Although we focused primarily on 72 hpf larvae, this reduction in size was evident by 48 hpf (data not shown). This phenotype was apparent in $sop^{-/-}$ larvae as well as nicotine-exposed wild-type larvae. This reduction in size along the dorsal/ventral axis has also been reported for another paralytic mutant $nic^{b107/b107}$, also known as the *nic1* mutant (van der Muelen et al., 2005). At the cross section-level, white muscle fibers of $sop^{-/-}$ larvae appeared very similar to white muscle fibers in stage matched *sop* sibling larvae, or wild-type larvae (Figs. 4A, B).

At the whole-mount level, the white muscle fibers appeared relatively normal in 72 hpf $sop^{-/-}$ larvae (Fig. 4C). However, in some instances, there was a slight disorganization in the region where fast muscle nuclei are located. The sarcomeres appeared to “unzip” in this region (data not shown), but this was rare when compared to the observations of “unzipping” sarcomeres seen in the slow muscle of $sop^{-/-}$ larvae. In the middle of the slow muscle fibers of $sop^{-/-}$ larvae, a characteristic “bubbling” was often apparent when larvae were analyzed in whole-mount (Fig. 4D). At high magnification, the sarcomeres appeared to be “unzipping” in the middle of the segments (Fig. 4D). This phenotype has also been observed for the slow muscle fibers of the *nic1* mutant, but in that study the fibers were not analyzed at 72 hpf. That analysis was performed at 24–48 hpf (Brennan et al., 2005).

Sofa potato paralytic zebrafish larvae: exposure to nicotine

We hypothesized that nicotine exposure would not further impact muscle development in $sop^{-/-}$ larvae. As $sop^{-/-}$ embryos are paralytic mutants, they never exhibit the spontaneous contractions of the musculature which occur in wild-type embryos as early as 18–19 hpf (Saint-Amant and Drapeau, 1998). Using this criteria (Teraoka et al., 2006), we were able to identify

and expose *sop*$^{-/-}$ *embryos* to nicotine as early as 21–22 hpf. Exposing *sop*$^{-/-}$ embryos to 30 μM nicotine caused no obvious deleterious abnormalities in muscle development (Fig. 5A, bottom, Fig. 6A, right). Slow muscle fibers in *sop*$^{-/-}$ larvae were not further impacted by the nicotine exposure when analyzed at the whole-mount level (Fig. 5A, bottom). On the other hand, the width of the slow muscle fibers (dorsal to ventral) which corresponds to sarcomere length was significantly reduced in nicotine-exposed *sop*$^{+/?}$ larvae (Figs. 5A top, 5B). At the level of cross-section analysis, fast muscle fibers were not affected by nicotine exposure in 72 hpf *sop*$^{-/-}$ larvae. In contrast, the fast muscle fibers in nicotine-exposed 72 hpf *sop*$^{+/?}$ larvae appeared to undergo a severe degeneration and looked very similar to the fast muscle fibers in 72 hpf *isl1* larvae exposed to nicotine (Fig. 6A, left, compare to Fig. 2C). Although *sop*$^{-/-}$ larvae were shorter in the dorsal/ventral axis when compared to siblings or wild-types, exposure to nicotine did not cause a further reduction in the size of *sop*$^{-/-}$ larvae (Figs. 6B, C, for comparison purposes see vertical reference bars in Figs. 4B and 6B).

Nicotine exposure in sop mutants alters motoneuron axonal pathfinding

In our previous study (Svoboda et al., 2002), *isl1* zebrafish were used to detect changes in cell differentiation as well as motoneuron axonal pathfinding. Unfortunately, we do not have the *sop* line crossed into *the isl1* line. Thus, in the following experiments utilizing *sop* mutants, zn5 was used to label secondary motoneuron axons. Prior to this, it was confirmed that zn5 could reliably detect the GFP-positive dorsal secondary motoneuron axons in *isl1* larvae (Figs. 7A–C). These dorsal projections were previously shown to be altered by nicotine exposure (Svoboda et al., 2002).

The zebrafish paralytic mutant known as *nic1* has inactive muscle, but motoneuron axonal development is normal in this mutant (Westerfield et al., 1990). Moreover, if *twi* mutants are injected with α-bungarotoxin to block their overactive skeletal muscle AChRs, the motoneuron axons in those mutants also develop normally (Lefebvre et al., 2004). Thus, it appears that functional muscle nAChRs are not necessarily required for normal motoneuron axonal pathfinding. If this were true, one would predict that motoneuron development would be normal in *sop*$^{-/-}$ larvae lacking skeletal muscle AChRs. Indications of normal motoneuron development in *sop* mutants has been documented (see Fig. 1 of Ono et al., 2001). In that study, the *isl1* line was crossed into the *sop* line allowing for motoneuronal morphology to be assessed in living larvae. As expected, there were no obvious abnormalities in the GFP-positive secondary motoneurons in the *sop*$^{-/-}$ larvae. The observations of Ono et al., 2001 were confirmed for *sop*$^{-/-}$ larvae where it was found that the axons of both primary and secondary motoneurons appeared normal when compared to stage matched siblings and wild-type larvae. Neither the primary nor secondary motoneuron axons exhibited ectopic branches or had severe deficiencies in targeting to the periphery in these mutants (Supplement Fig. 1).

Since nicotine exposure had no further obvious consequences on muscle development in *sop*$^{-/-}$ larvae and given that the motoneuron axons in *sop*$^{-/-}$ larvae appeared normal, we felt that we could reliably use these paralytic mutants to determine if nicotine exposure directly impacts CNS development. In utilizing *sop* mutants, we hoped to eliminate any contribution that muscle degeneration or over-stimulated skeletal muscle AChRs would potentially have on motoneuron development. Upon exposure to 15–30 μM nicotine, secondary motoneuron axons of *sop*$^{-/-}$ larvae made pathfinding errors (Figs. 8A, B).

Dorsal projecting secondary motoneuron axons in zebrafish larvae associate with nAChRs

We previously demonstrated that nicotine-induced alterations in secondary motoneuron cell biology could be reversed if the embryos were pre-treated with DHβE, an α4/β2 nAChR antagonist (Svoboda et al., 2002). This suggested to us that motoneurons could possibly express an α4/β2 nAChR. If these neuronal nicotinic receptors were modulated by nicotine exposure,

this could influence axonal pathfinding. Since we now have demonstrated that nicotine directly acts on the CNS to cause pathfinding errors of secondary motoneuron axons, this possibility becomes even more intriguing.

We designed a polyclonal antibody against the zebrafish β2 nAChR subunit. We chose to make an antibody against this subunit because it is a component of α4/β2 nAChRs that we implicated in underlying nicotine-induced alterations in motoneurons and because others have demonstrated via binding studies that α4/β2 nAChRs are likely expressed in embryonic zebrafish (Zirger et al., 2003).

Using western blot analysis, our zebrafish anti-β2 nAChR antibody did not reliably detect a protein of the appropriate molecular weight for the β2 nAChR subunit. As is the case for many commercially available nAChR receptor antibodies, they often only work in non-denaturing conditions such as immunohistochemistry. Using whole animal immunohistochemistry, the anti-β2 nAChR antibody labeled a population of spinal mechanosensory neurons known as Rohon–Beard neurons in 36 hpf embryos. These neurons can be identified on the basis of their size and position in dorsal spinal cord (Fig. 9A, top). To determine if we could effectively knockdown β2 nAChR protein expression, a morpholino (MO) was designed to repress β2 nAChR protein expression. In 36 hpf β2 nAChR MO-injected embryos, the β2 nAChR expression was reduced in the dorsal spinal cord (Fig. 9A, bottom right). In control MO-injected embryos, β2 nAChR labeling was indistinguishable from the non-injected animals (Fig. 9A, bottom left). Collectively these results indicate that we can readily detect and repress embryonic β2 nAChR expression.

The distribution of the β2 nAChR subunit in 72 hpf *isl1* zebrafish larvae was detected via immunohistochemistry. In our previous study, we showed that dorsal projecting secondary motoneuron axons in nicotine-exposed embryos exhibited pathfinding errors (see Fig. 9 of Svoboda et al., 2002). In 72 hpf *isl1* larvae, expression of the β2 nAChR subunit appeared tightly associated with axons extending from the main GFP-positive dorsal nerve bundle (Figs. 9B, C). The same analysis was also performed in larvae using the zn5 antibody to label secondary motoneuron axons. β2 nAChR subunit expression was found to be associated with zn5 positive motoneuron axons exiting the ventral root and turning dorsally. The β2 nAChR subunit did not appear to be associated with the zn5 positive ventral projecting axons (data not shown).

If an α4/β2 nAChR is associated with motoneuron axons, a specific agonist of this receptor subtype should alter axonal pathfinding in a similar manner to nicotine when embryos are exposed to the agonist. Exposure of wild-type or *sop*$^{-/-}$ embryos to epibatidine (125 nM–1 μM) caused axon pathfinding errors (Figs. 10A–C). Exposure of embryos to the highest concentrations caused dorsal projecting secondary motoneuron axons to stall before entering the periphery (Fig. 10A, top). At the lowest concentrations of epibatidine, dorsal projecting secondary motoneuron axons extended dorsally, but still exhibited pathfinding errors (Figs. 10A, bottom, Fig. 10B, Fig. 10C). At the middle of the concentration range, the dorsal projecting axons often had ectopic branches appearing forked (Fig. 10A, middle). At both high and low epibatidine concentrations the dorsal axons were affected more than the ventrally projecting axons. When *sop*$^{-/-}$ embryos were exposed to epibatidine, the pathfinding of secondary motoneuron axons was altered by the larval stage of development (Fig. 10D). As *sop* mutants lack muscle ACh receptors, the epibatidine mediated effect is likely a direct effect on the CNS.

Discussion

When a pregnant woman smokes, she invariably exposes her unborn child to nicotine and numerous other chemicals contained in cigarette smoke. It has been estimated that that the unborn fetus can be exposed to nicotine levels ranging between to 0.6–6 μM (Zhao and Reece, 2005). In this situation as well as in other developing vertebrates, nicotine can act as a potent teratogen and influence neuronal development and subsequent function (Paz et al., 2007; Zhao and Reece, 2005; Izrael et al., 2004; Slotkin, 2004; Everekliogl u et al., 2003).

We are using the zebrafish as a model system to study nicotine toxicity that arises during development. We previously reported that nicotine exposure alters secondary motoneuron development and axonal pathfinding in zebrafish (Svoboda et al., 2002). In that work, the muscle development in nicotine-exposed larvae was not rigorously analyzed as they were paralyzed. We hypothesized that the mechanism of paralysis was likely due to the activation and subsequent desensitization of the muscle-specific AChRs by chronic nicotine exposure. However, it remained plausible that nicotine could actually be causing muscle degeneration (Wecker et al., 1978; Leonard and Salpeter, 1979). If this were the case, then any abnormal motoneuron development could be a downstream consequence of muscle degeneration. This has precedent in studies where aberrant zebrafish muscle development altered motoneuron development in parallel.

The concentrations of nicotine used in this study at first glance may seem high, but we are reporting waterborne concentrations, not embryonic doses, and we suspect that only a fraction of the nicotine is getting into the embryo. This is based on the premise that prior to our 2002 publication, dose response (concentration) experiments were conducted to evaluate the range of nicotine required to alter overall zebrafish development. Using an exposure protocol similar to one described herein, concentrations between 0.1 and 50 μM did not lead to detectable embryonic malformations or mortality, and the exposed embryos as they transitioned to the larval stage of development were morphologically indistinguishable from non-exposed controls (unpublished observations). However, a continuous 100 μM water-borne nicotine exposure resulted in approximately 40% embryonic mortality at 96 hpf (unpublished observations). Since our goal is to evaluate sub-lethal developmental nicotine responses, the upper exposure limit was set at ~30 μM nicotine. At this waterborne concentration, embryos become functionally paralyzed when exposed to nicotine from 22–72 hpf. However, these nicotine-exposed embryos survive well into adulthood (Menelaou and Svoboda, 2009).

In mammalian studies utilizing embryonic explants, concentrations between 0.6 μM and 6 μM nicotine typically result in embryonic deformities. Embryonic lethality occurred in those explants when they were exposed to 6 μM nicotine (Zhao and Reece, 2005). In the present study, we built upon our previous published work where we showed that nicotine exposure altered motoneuron development in zebrafish. We now demonstrate that nicotine can impact muscle and nervous system development independently.

Chronic nicotine exposure and muscle development

Nicotine exposure in embryonic zebrafish resulted in muscle degeneration by 72 hpf. This was likely due to over-activation of muscle-specific AChRs by chronic nicotine stimulation. Our findings are consistent with other data from zebrafish and transgenic mice where mutant muscle AChR channels with prolonged over-activation lead to subsequent muscle degeneration and myopathy. It is possible that an increase in muscle calcium levels causes this degeneration. Nicotine can also cause desensitization of the muscle receptors but desensitization is not likely to cause the myopathy. *sop*$^{-/-}$ embryos lacking muscle AChRs did not exhibit myopathy when exposed to nicotine. Thus, in non-mutant embryos, it seems that exposure to chronic nicotine is over-activating muscle AChRs. Receptor over-activation and the concomitant dramatic rise

in muscle calcium could cause the myopathy via excitotoxic mechanisms (Engel et al., 1982, 2003; Gomez et al., 2002).

These observations are also consistent with data obtained from zebrafish mutants lacking acetylcholinesterase (AChE) which is the enzyme that breaks down acetylcholine. In those AChE mutants, excess ACh may over-stimulate the muscle AChRs resulting in degenerated muscle (Behra et al., 2002).

In this study we also gained further insight into the potential roles of nicotinic acetylcholine receptors in vertebrate muscle development. One of the observations made in the current study was that fast muscle development was relatively normal in *sop*$^{-/-}$ larvae not exposed to nicotine. The F310 immunohistochemistry revealed that fast muscle fibers were intact and were well-organized. At the cross-section level, the fast muscle fibers also looked normal at 72 hpf.

Others have evaluated the role that muscle-specific AChRs play in slow muscle development. For example, sarcomere width and myofibril length required functional muscle-specific AChRs (Brennan et al., 2005). In our study, slow muscle in *sop*$^{-/-}$ larvae was indeed present, but its morphology was altered. Our results are consistent with the studies of Brennan et al. (2005) that reported disrupted *slow* muscle myofiber organization in the *nic1* paralytic mutant. They detected this disorganization in embryos as old as 48 hpf.

Another unique observation made in this study was that both the nicotine-exposed (30 μM) and *sop*$^{-/-}$ larvae were smaller than stage matched *sop*$^{+/?}$ or wild-type larvae. This size reduction has been reported by another group studying the *nic1* mutant zebrafish (van der Muelen et al., 2005), and is not likely related to axonal pathfinding errors or degenerated muscle because in the *sop* mutants, muscle and motoneuron axons are present and appear normal (our work and Ono et al., 2001). In nicotine-exposed wild-type larvae, the motoneuron axons and muscle are altered. However, both nicotine-exposed wild-type and *sop*$^{-/-}$ larvae were similar in length along the dorsal/ventral axis.

The reduced size may be related to a lack of movement. This conclusion is further supported by data presented under supplemental Fig. 2. All of the larval types (i.e., *sop*$^{-/-}$, nicotine-exposed wild-types, etc.) presented in this paper were compared to wild-type embryos raised in 0.006%–0.01% tricaine, an anesthetic that blocks sodium channel function. Zebrafish embryos exposed to tricaine from 22–72 hpf did not move by 72 hpf; however, their muscle at the cross-section level appeared normal. They were approximately the same size as the *sop* mutants and nicotine-exposed wild-type larvae. We conclude that the size reduction reported in this paper may not be related to muscle degeneration or abnormal axonal pathfinding, but may simply be an effect of prolonged paralysis consistent with observations of van der Muelen et al., 2005.

Nicotine interacts directly with the CNS to alter motoneuron axon pathfinding

Nicotine directly influences CNS development. We used the *sop* paralytic mutant, which lacks only muscle ACh receptors but has normal axonal pathfinding, to demonstrate that nicotine and epibatidine exposure disrupts axonal pathfinding. This indicates that activation of nicotinic receptors on CNS elements, possibly the motoneurons themselves, mediate the pathfinding errors. We are not the first group to demonstrate that motoneuron axonal targeting is normal when the post-synaptic muscle apparatus is silent. Westerfield et al. (1990) characterized motoneuron axons in a paralytic zebrafish mutant lacking skeletal muscle nAChRs. The axons were normal. When α-bungarotoxin was injected into zebrafish embryos to block muscle activity, the axons were normal (Lefebvre et al., 2004). However, when *sop*$^{-/-}$ embryos were exposed to nicotine or epibatidine, their motoneuron axons exhibited pathfinding errors by 72 hpf.

Based on pharmacologic inhibition data from our previous work (Svoboda et al., 2002), we hypothesized that motoneurons should express nAChRs, possibly α4/β2 nAChRs. Consistent with this, the β2 nAChR subunit was detected in zebrafish and its expression was associated with motoneurons in 72 hpf larvae. This finding, coupled with the results of the epibatidine exposures, suggests that β2 nAChR subunits may form functional receptors with "α4-like" subunits or other alpha nAChR subunits in zebrafish. Modulation of these receptors likely caused the pathfinding errors in dorsal projecting motoneuron axons in wild-type and *sop*$^{-/-}$ larvae.

It is possible that endogenous acetylcholine may act as a signaling molecule in a non-synaptic fashion to guide normal motoneuron axon development in zebrafish. Within this context, activation of nAChRs has been shown to regulate neurite outgrowth in chick ciliary ganglion neurons (Pugh and Berg, 1994) and in *Xenopus* spinal neurons (Zheng et al., 1994). In the ciliary ganglion, application of either nicotine or acetylcholine caused a retraction of neurite outgrowth that was dependent on external calcium. In the *in vivo* paradigm, it is hypothesized that neurite retraction may be related to activation of nAChRs associated with the nerve terminal (Pugh and Berg, 1994).

In the zebrafish system, it may be the case that nicotine exposure over-activates nAChRs and ultimately raises intracellular calcium levels in the neurite. If calcium homeostasis was disrupted within the growth cone, this could cause the axons to target into the periphery in an unorganized manner, or potentially cause them to stall and retract (Pugh and Berg, 1994; Gomez and Spitzer, 1999). Another possibility is that the exposure to nicotine desensitizes the expression of nAChRs associated with the motoneuron axons targeting to the periphery. If this occurred, those receptors would not be able to respond to endogenous acetylcholine signals and the axons would potentially target to the periphery with no direction or guidance. This assumes that acetylcholine is acting non-synaptically to modulate neurite extension in the developing zebrafish. We are currently investigating these possibilities.

Supplementary Material

Refer to Web version on PubMed Central for supplementary material.

Acknowledgments

This work was supported by grants from the Louisiana Board of Regents LEQSF(2005-08)-RD-A-11 and the NIH/National Institute of Environmental Health Sciences ES016513 (KRS) and P30-ES00210 (Oregon State University, RLT). We thank Ms. Robin Pollet for providing expert zebrafish care and embryo management. We thank Chris Cullom for helping with the epibatidine experiments and we thank Ms. Ying Xiao of the Socolofsky Microscopy Facility at LSU for expert histology work, tissue preparation, and sectioning.

References

Behra M, Cousin X, Bertrand C, Vonesch JL, Biellmann D, Chatonnet A, Strahle U. Acetylcholinesterase is required for neuronal and muscular development in the zebrafish embryo. Nat. Neurosci 2002;5:111–118. [PubMed: 11753420]

Birely J, Schneider VA, Santana E, Dosch R, Wagner DS, Mullins MC, Granato M. Genetic screens for genes controlling motor nerve-muscle development and interactions. Dev. Biol 2005;280:162–176. [PubMed: 15766756]

Brennan C, Mangoli M, Dyer CEF, Ashworth R. Acetylcholine and calcium signaling regulates muscle fibre formation in the zebrafish embryo. J. Cell. Sci 2005;118:5181–5190. [PubMed: 16249237]

Chow HES, Cheng SH. Cadmium affects muscle type development and axon growth in zebrafish embryonic somitogenesis. Toxicol. Sci 2003;73:149–159. [PubMed: 12700413]

Dahm LM, Landmesser LT. The regulation of intramuscular nerve branching during normal development and following activity blockade. Dev. Biol 1988;130:621–644. [PubMed: 3058544]

Devoto SH, Melancon E, Eisen JS, Westerfield M. Identification of separate slow and fast muscle precursor cells in vivo, prior to somite formation. Development 1996;122:3371–3380. [PubMed: 8951054]

Engel AG, Lambert EH, Mulder DM, Torres CF, Sahashi K, Bertorini TE, Whitaker JN. A newly recognized congenital myasthenic syndrome attributed to a prolonged open time of the acetylcholine-induced ion channel. Ann. Neurol 1982;11:553–569. [PubMed: 6287911]

Engel AG, Ohno K, Sine SM. Congenital myasthenic syndromes: multiple molecular targets at the neuromuscular junction. Ann. N.Y. Acad. Sci 2003;998:138–160. [PubMed: 14592871]

Evereklioglu C, Ozkiriş A, Alaşehirli B, Sari I, Güldür E, Cengiz B, Kontaş O. Effect of gestational nicotine treatment on newborn rat retina: a histopathological and morphometric analysis. Ophthalmic Physiol. Opt 2003;23:527–533. [PubMed: 14622356]

Gomez TM, Spitzer NC. In vivo regulation of axon extension and pathfinding by growth-cone calcium transients. Nature 1999;6717:350–355. [PubMed: 9950427]

Gomez CM, Maselli RA, Groshong J, Zayas R, Wollmann RL, Cens T, Charnet P. Active calcium accumulation underlies severe weakness in a panel of mice with slow-channel syndrome. J. Neurosci 2002;22:6447–6457. [PubMed: 12151524]

Higashijima S, Hotta Y, Okamoto H. Visualization of cranial motor neurons in live transgenic zebrafish expressing green fluorescent protein under the control of the Islet-1 promoter/enhancer. J. Neurosci 2000;20:206–218. [PubMed: 10627598]

Izrael M, Van der Zee EA, Slotkin TA, Yanai J. Cholinergic synaptic signaling mechanisms underlying behavioral teratogenicity: effects of nicotine, chlorpyrifos, and heroin converge on protein kinase C translocation in the intermedial part of the hyperstriatum ventrale and on imprinting behavior in an avian model. J. Neurosci. Res 2004;78:499–507. [PubMed: 15470723]

Kawahara A, Chien CB, Dawid IB. The homeobox gene mbx is involved in eye and tectum development. Dev. Biol 2002;248:107–117. [PubMed: 12142024]

Landmesser LT. The relationship of intramuscular nerve branching and synaptogenesis to motoneuron survival. J. Neurobiol 1992;23:1131–1139. [PubMed: 1469380]

Lefebvre JL, Ono F, Puglielli C, Seidner G, Franzini-Armstrong C, Brehm P, Granato M. Increased neuromuscular activity causes axonal defects and muscular degeneration. Development 2004;131:2605–2618. [PubMed: 15128655]

Leonard JP, Salpeter MM. Agonist-induced myopathy at the neuromuscular junction is mediated by calcium. J. Cell. Biol 1979;82:811–819. [PubMed: 511934]

Menelaou E, Svoboda KR. Secondary motoneurons in juvenile and adult zebrafish: Axonal pathfinding errors caused by embryonic nicotine exposure. J. Comp. Neurol 2009;512:305–322. [PubMed: 19006183]

Ono F, Higashijima S, Shcherbatko A, Fetcho JR, Brehm P. Paralytic zebrafish lacking acetylcholine receptors fail to localize rapsyn clusters to the synapse. J. Neurosci 2001;21:5439–5448. [PubMed: 11466415]

Paz R, Barsness B, Martenson T, Tanner D, Allan AM. Behavioral teratogenicity induced by nonforced maternal nicotine consumption. Neuropsychopharmacology 2007;32:693–699. [PubMed: 16554741]

Pineda RH, Svoboda KR, Wright MA, Taylor AD, Novak AE, Gamse JT, Eisen JS, Ribera AB. Knockdown of Nav1.6a Na+ channels affects zebrafish motoneuron development. Development 2006;133:3827–3836. [PubMed: 16943272]

Pittman R, Oppenheim RW. Cell death of motoneurons in the chick embryo spinal cord. IV. Evidence that a functional neuromuscular interaction is involved in the regulation of naturally occurring cell death and the stabilization of synapses. J. Comp. Neurol 1979;187:425–446. [PubMed: 489787]

Pugh PC, Berg DK. Neuronal acetylcholine receptors that bind alpha-bungarotoxin mediate neurite retraction in a calcium-dependent manner. J. Neurosci 1994;14:889–896. [PubMed: 8301367]

Saint-Amant L, Drapeau P. Time course of the development of motor behaviors in the zebrafish embryo. J. Neurobiol 1998;37:622–632. [PubMed: 9858263]

Sherwood, L. Fundamentals of Physiology. 2nd ed.. St. Paul: West Publishing Company; 1995.

Slotkin TA. Cholinergic systems in brain development and disruption by neurotoxicants: nicotine, environmental tobacco smoke, organophosphates. Toxicol. Appl. Pharmacol 2004;198:132–151. [PubMed: 15236950]

Svoboda KR, Linares AE, Ribera AB. Activity regulates programmed cell death of zebrafish Rohon-Beard neurons. Development 2001;128:3511–3520. [PubMed: 11566856]

Svoboda KR, Vijayaraghaven S, Tanguay RL. Nicotinic receptors mediate changes in spinal motoneuron development and axonal pathfinding in embryonic zebrafish exposed to nicotine. J. Neurosci 2002;22:10731–10741. [PubMed: 12486166]

te Kronnie G. Axial muscle development in fish. Basic Appl. Myol 2000;10:261–267.

Teraoka H, Urakawa S, Nanba S, Nagai Y, Dong W, Imagawa T, Tanguay RL, Svoboda K, Handley-Goldstone HM, Stegeman JJ, Hiraga T. Muscular contractions in the zebrafish embryo are necessary to reveal thiuram-induced notochord distortions. Toxicol. Appl. Pharmacol 2006;212:24–34. [PubMed: 16051294]

van der Muelen T, Schipper H, van Leeuwen JL, Kranenbarg S. Effects of decreased muscle activity on developing axial musculature in nic^{b107} mutant zebrafish (*Danio rerio*). J. Exp. Biol 2005;208:3675–3687. [PubMed: 16169945]

van Eeden FJ, Granato M, Schach U, Brand M, Furutani-Seiki M, Haffter P, Hammerschmidt M, Heisenberg CP, Jiang YJ, Kane DA, Kelsh RN, Mullins MC, Odenthal J, Warga RM, Allende ML, Weinberg ES, Nüsslein-Volhard C. Mutations affecting somite formation and patterning in the zebrafish, *Danio rerio*. Development 1996;123:153–164. [PubMed: 9007237]

van Raamsdonk W, Pool CW, te Kronnie G. Differentiation of muscle fiber types in the teleost *Brachydanio rerio*. Anat. Embryol. Berl 1978;153:137–155. [PubMed: 677468]

Wecker L, Kiauta T, Dettbarn WD. Relationship between acetylcholinesterase inhibition and the development of a myopathy. J. Pharmacol. Exp. Ther 1978;206:97–104. [PubMed: 660561]

Westerfield, M. The Zebrafish Book: A Guide for the Laboratory Use of Zebrafish (*Danio Rerio*). Eugene: University of Oregon Press; 1995.

Westerfield M, Liu DW, Kimmel CB, Walker C. Pathfinding and synapse formation in a zebrafish mutant lacking functional acetylcholine receptors. Neuron 1990;4:867–874. [PubMed: 2361010]

Zeller J, Granato M. The zebrafish diwanka gene controls an early step of motor growth cone migration. Development 1999;126:3461–3472. [PubMed: 10393124]

Zeller J, Schneider V, Malayaman S, Higashijima S, Okamoto H, Gui J, Lin S, Granato M. Migration of zebrafish spinal motor nerves into the periphery requires multiple myotome-derived cues. Dev. Biol 2002;252:241–256. [PubMed: 12482713]

Zhao Z, Reece EA. Nicotine-induced embryonic malformations mediated by apoptosis from increasing intracellular calcium and oxidative stress. Birth Defects Res. B. Dev. Reprod. Toxicol 2005;74:383–391. [PubMed: 16193507]

Zheng JQ, Felder M, Connor JA, Poo MM. Turning of nerve growth cones induced by neurotransmitters. Nature 1994;368:140–144. [PubMed: 8139655]

Zirger J, Beattie CE, McKay DB, Boyd RT. Cloning and expression of zebrafish neuronal nicotinic acetylcholine receptors. Gene Expression Patterns 2003;3:747–754. [PubMed: 14643683]

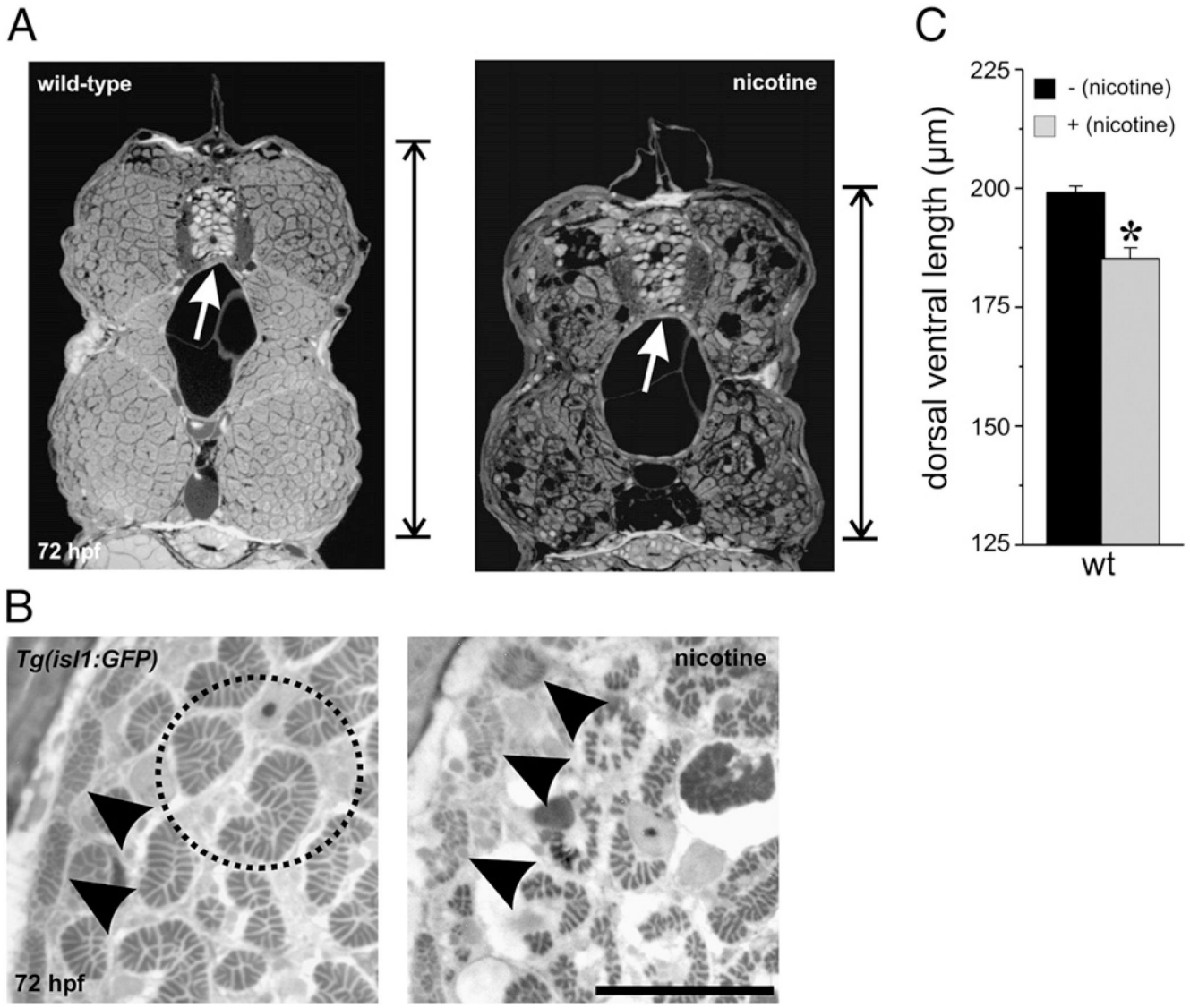

Fig. 1.

Nicotine exposure causes muscle degeneration in developing zebrafish. (A) Photomicrographs of cross-sections obtained from the mid trunk region of a wild-type larva (left) and wild-type larva exposed to nicotine from 22–72 hpf (right). These black and white images have been inverted for visualization purposes. The nicotine-exposed larva is smaller than the non-exposed larva in the dorsal/ventral axis. The vertical line at the right of the images denotes the length along the dorsal/ventral axis that was measured for quantification purposes. The white arrows point to the spinal cord. (B) Magnified views of cross-sections from non-exposed and nicotine-exposed *isl1* larvae. Black arrowheads point to slow muscle fibers at the periphery. Note in the nicotine-exposed larva that the slow muscle fibers are disorganized. The fast muscle fibers (black dotted circle highlights a few in the non-exposed larva) are also disorganized and smaller in size in the nicotine-exposed larva. (C) Quantification of dorsal/ventral axis lengths in 72 hpf wild-type larvae. Wild-type (n = 9 larvae, 199.1 ± 1.29 μm), nicotine-exposed wild-type (n = 9 larvae; 185.2 ± 2.29 μm). Asterisk denotes significance with a p value <0.05. Scale bar = 20 μm.

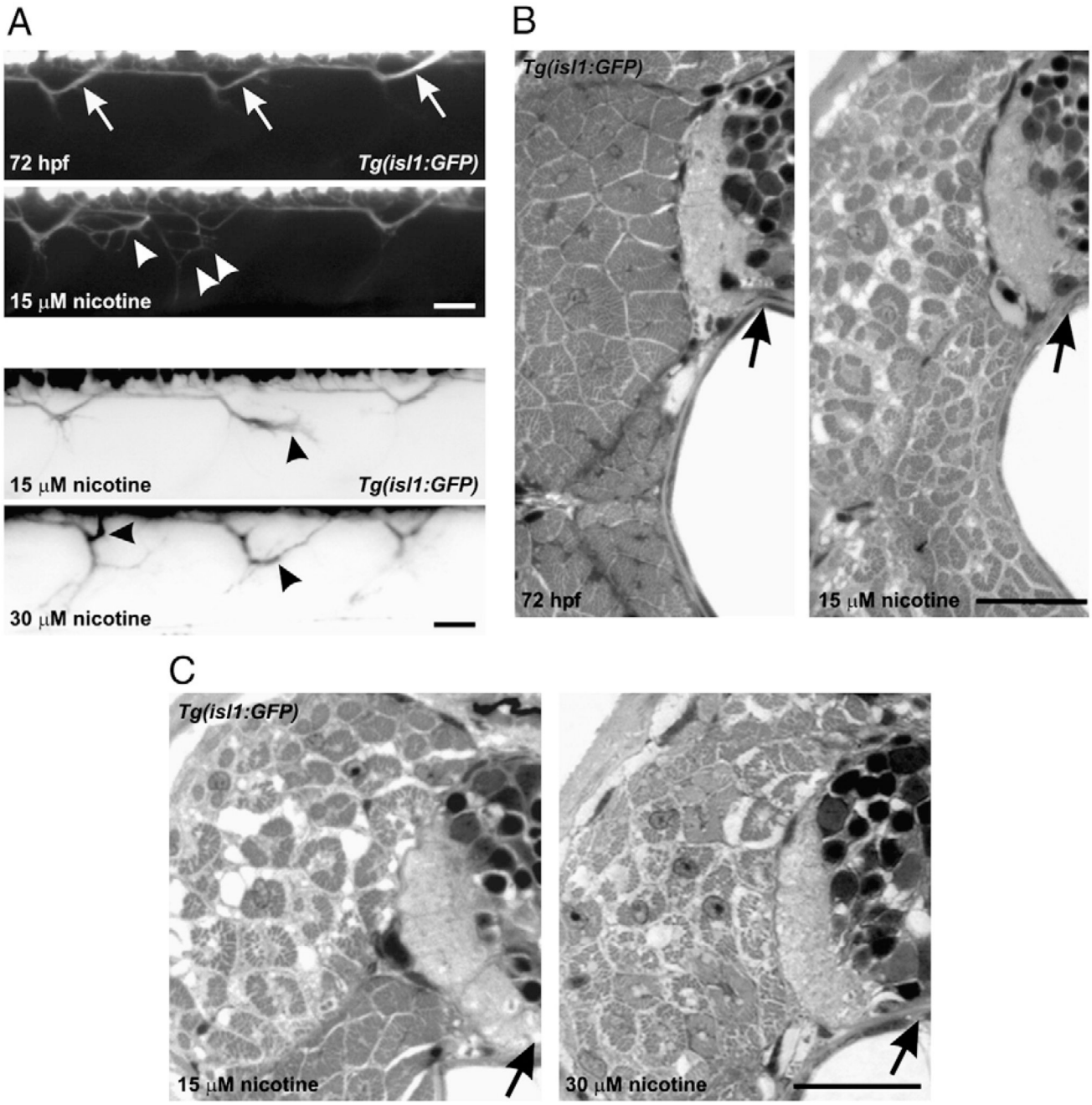

Fig. 2.

Motoneuron axonal pathfinding errors and muscle abnormalities in larvae exposed to nicotine. (A) Four photomicrographs of 72 hpf, *isl1* living larvae. At the top is a control larva ($n = 7$), and the remaining are photomicrographs obtained from larvae exposed to 15 μM ($n = 6$) or 30 μM nicotine ($n = 7$). The top two black and white panels correspond to the muscle panels shown in B. The bottom two "inverted" images correspond to the muscle panels in C. Arrows in the control larva denote secondary motoneuron axons which exit ventral spinal cord and turn to project to the dorsal musculature. In the 15 μM nicotine-exposed larvae, those axons which project to the dorsal musculature have abnormal trajectories (white arrowheads and black arrowhead). In the 30 μM nicotine-exposed larva, black arrowheads point to abnormally

projecting dorsal axons. (B) Photomicrographs of cross-sections through spinal cord and muscle for those individual fish shown in two top panels in A. Left, the muscle fibers in the non-exposed larva appear normal. The black arrow is pointing to spinal cord. Right, image of the 15 μM nicotine-exposed larvae shown in panel A. The medial muscle fibers comprised of fast muscle fibers have abnormal morphologies appearing to be smaller and possibly degenerated. The black arrow is pointing to spinal cord. (C) Photomicrographs of cross-sections obtained from the 15 and 30 μM nicotine-exposed larvae shown in A, inverted images. Black arrows point to spinal cord. Scale bars = 20 μm.

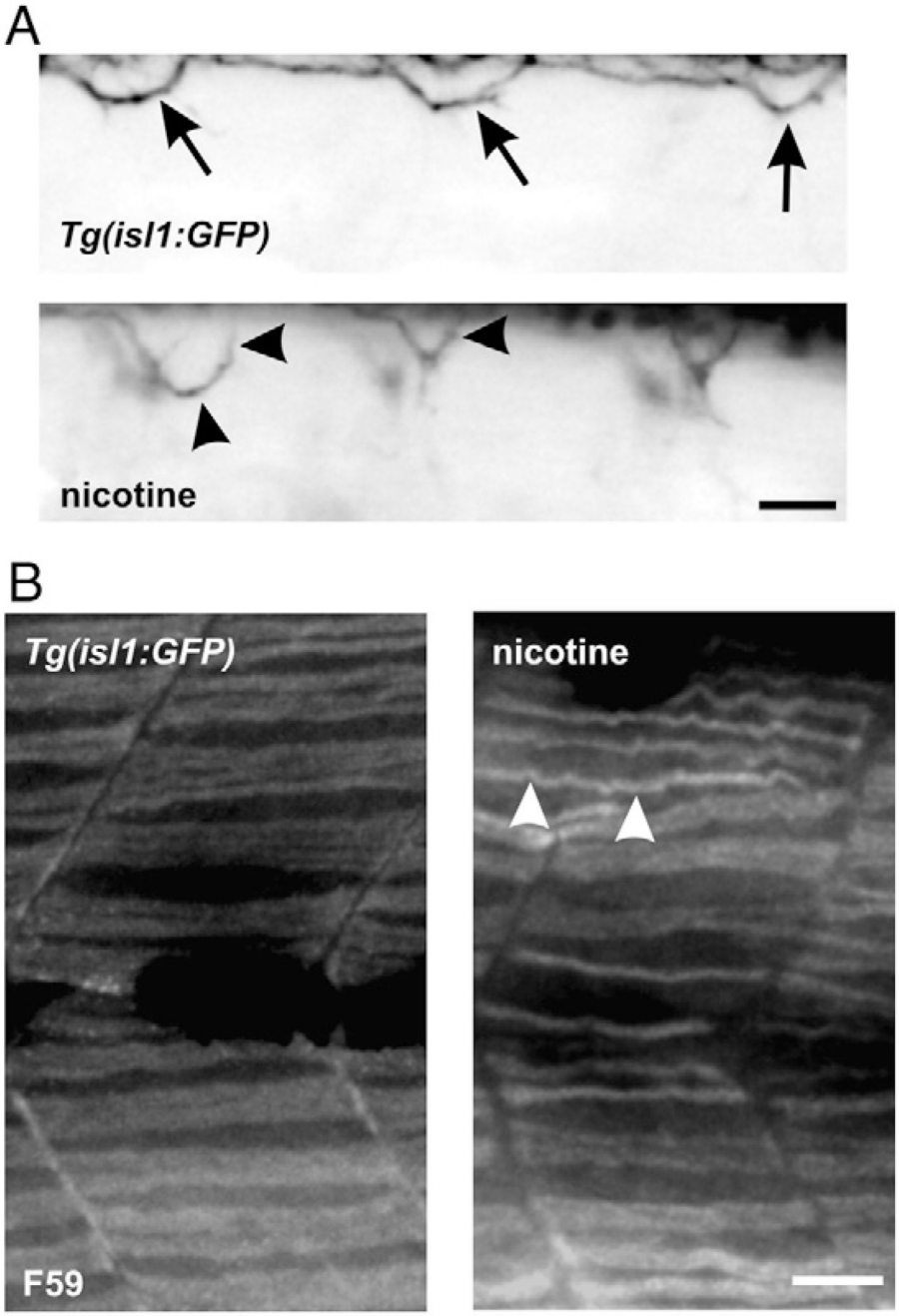

Fig. 3.

Motoneuron axonal pathfinding errors and muscle abnormalities in larvae exposed to nicotine: slow muscle immunohistochemistry. (A) Photomicrographs of 72 hpf, *isl1* larvae. At the top is an image of a control larva. At the bottom is an image of a nicotine-exposed (30 μM) larva. Arrows in the control larva denote secondary motoneuron axons which project to the dorsal musculature. In the nicotine-exposed larva, those axons which project to the dorsal musculature do no not target correctly (black arrowheads). (B) Photomicrographs of muscle fibers from the larvae shown in A labeled with the F59 antibody to detect slow muscle fibers at the whole-mount level. The slow muscle fibers are thinner in the nicotine-exposed *isl1* larva (n = 11)

when compared to control (n = 10). Note that some of the fibers cross over to the next segment in the exposed larva (white arrowheads). Scale bars = 20 μm.

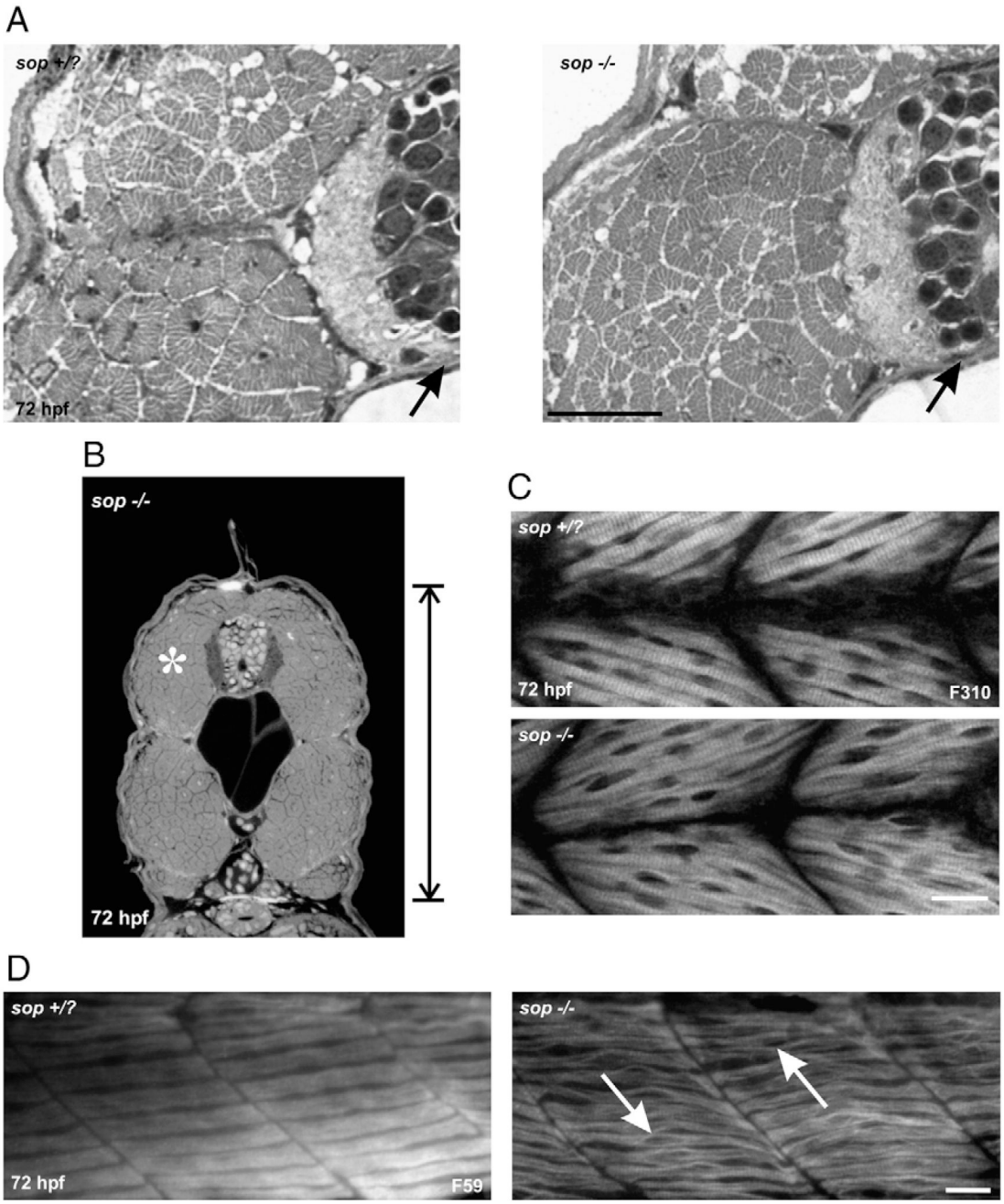

Fig. 4.

Muscle fiber development in 72 hpf *sop* mutants. (A) Photomicrographs from a region of cross-sections obtained from a 72 hpf $sop^{+/?}$ larva (left) and a 72 hpf $sop^{-/-}$ larva (right). In each, the black arrows point to the spinal cord. The fast muscle fibers in the mutant appear very similar to those fast fibers in the sibling. (B) Photomicrograph of a cross-section obtained from the mid trunk region of a 72 hpf $sop^{-/-}$ larva. The white asterisk denotes the region of interest that is presented in A. (C) Photomicrographs of a 72 hpf $sop^{+/?}$ larva (top) and a 72 hpf $sop^{-/-}$ larva (bottom) labeled with the antibody F310 to detect fast muscle fibers. (D) Photomicrographs of a 72 hpf $sop^{+/?}$ larva (left) and a 72 hpf $sop^{-/-}$ larva (right) labeled with

the antibody F59 to detect slow muscle fibers. In the mutant, the fibers appear to unzip at the middle of the muscle segment (white arrows). Scale bars = 20 μm.

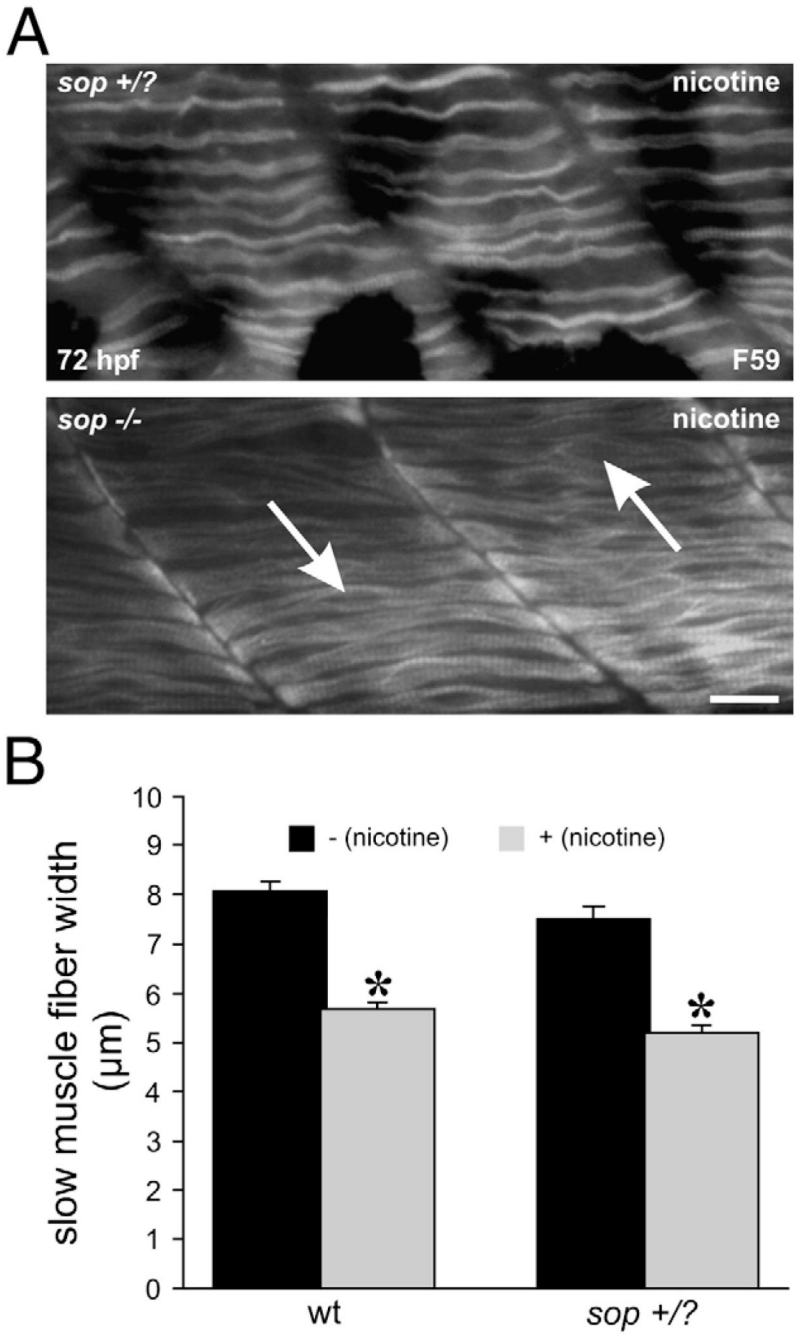

Fig. 5.

Nicotine exposure in 72 hpf *sop* larvae, slow muscle and analysis of whole mounts. (A) Photomicrographs of a 72 hpf $sop^{+/?}$ larva exposed to nicotine (top) and a 72 hpf $sop^{-/-}$ larva exposed to nicotine (bottom). Both larvae were labeled with the antibody F59 to detect slow muscle fibers. In the nicotine-exposed $sop^{-/-}$ larva, the fibers resemble slow muscle fibers of the 72 hpf $sop^{-/-}$ larva shown under Fig. 4D. The fibers still appear to unzip at the middle of the muscle segment (white arrows) in the nicotine-exposed $sop^{-/-}$ larva. The slow muscle fibers in the nicotine-exposed $sop^{+/?}$ larva are thin compared to those in the non-exposed $sop^{+/?}$ larva shown under Fig. 4D. (B) Slow muscle fiber width (dorsal/ventral) was quantified for 72 hpf wild-type, nicotine-exposed wild-type, $sop^{+/?}$, and nicotine-exposed $sop^{+/?}$ larvae. Nicotine

exposure (30 μM) caused a significant reduction in muscle fiber width in both wild-type and *sop*$^{+/?}$ larvae. Fiber widths: wild-type (*n* = 5 larvae, 8.08 ± 0.18 μm, *n* = 67 fibers); nicotine-exposed wild-type (*n* = 5 larvae; 5.68 ± 0.14 μm, n = 66 fibers), *sop*$^{+/?}$ (*n* = 5 larvae, 7.52 ± 0.24 μm, *n* = 55 fibers), nicotine-exposed *sop*$^{+/?}$ (*n* = 5 larvae, 5.21 ± 0.15 μm, *n* = 54 fibers). Asterisks denote significance with a *p* value <0.05. Scale bar = 20 μm.

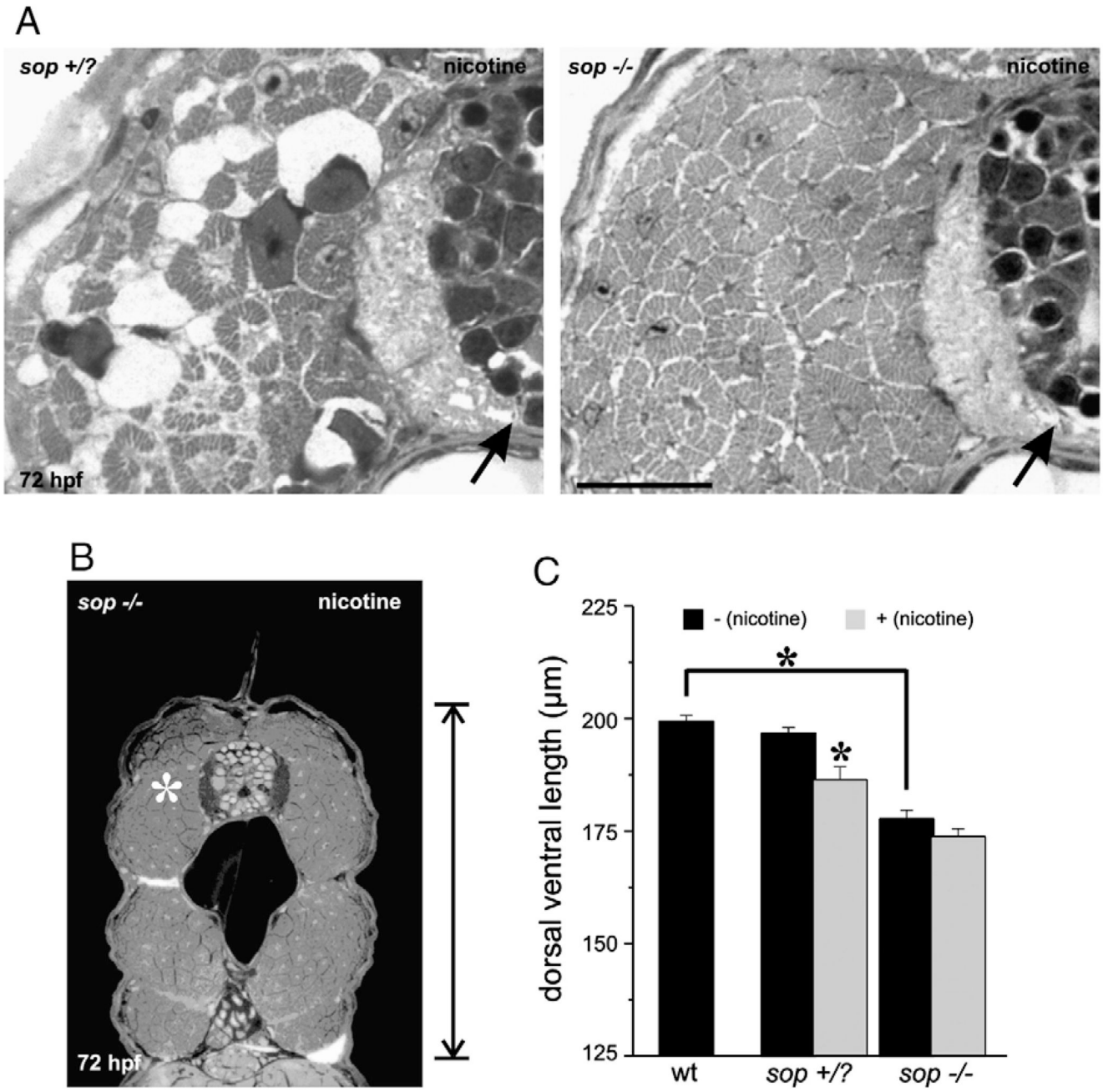

Fig. 6.

Nicotine exposure in 72 hpf *sop* larvae, fast muscle cross-section analysis. (A) Photomicrographs of a portion of cross-sections obtained from a 72 hpf $sop^{+/?}$ larva (left) and a 72 hpf $sop^{-/-}$ larva (right). Both were exposed to nicotine. In each, the black arrows point to the spinal cord. The fast muscle fibers in the $sop^{+/?}$ larva appear degenerated as a result of being exposed to 30 µM nicotine. Nicotine exposure (30 µM) did not cause muscle degeneration in the mutant. (B) Photomicrograph of a cross-section obtained from the mid trunk region of a 72 hpf $sop^{-/-}$ larva that was exposed to 30 µM nicotine. White asterisk denotes region of interest that was focused on in A. (C) Quantification of dorsal/ventral axis lengths in 72 hpf larvae. Nicotine exposure resulted in a shortened dorsal/ventral axis in $sop^{+/?}$ larvae.

Sop$^{-/-}$ larvae not exposed to nicotine were also significantly shorter than stage matched wild-type (see Fig. 1C for numbers) or *sop*$^{+/?}$ larvae. Nicotine exposure did not cause a further shortening of the dorsal/ventral axis in *sop*$^{-/-}$ larvae. Dorsal/ventral axis lengths: *sop*$^{+/?}$ (n = 26 larvae, 196.86 ± 1.28 μm), nicotine-exposed *sop*$^{+/?}$ (n = 13 larvae, 186.59 ± 2.83 μm), *sop*$^{-/-}$ (n = 7 larvae, 177.85 ± 1.92 μm), nicotine-exposed *sop*$^{-/-}$ (n = 10 larvae, 173.94 ± 1. 71 μm). Asterisks denote significance with a p value <0.05. Note that the data presented for wild-type larvae are plotted to allow for direct comparison with *sop*$^{+/?}$ and *sop*$^{-/-}$ larvae. The quantification of the wild-type data is presented under Fig. 1C. Scale bar in A = 20 μm.

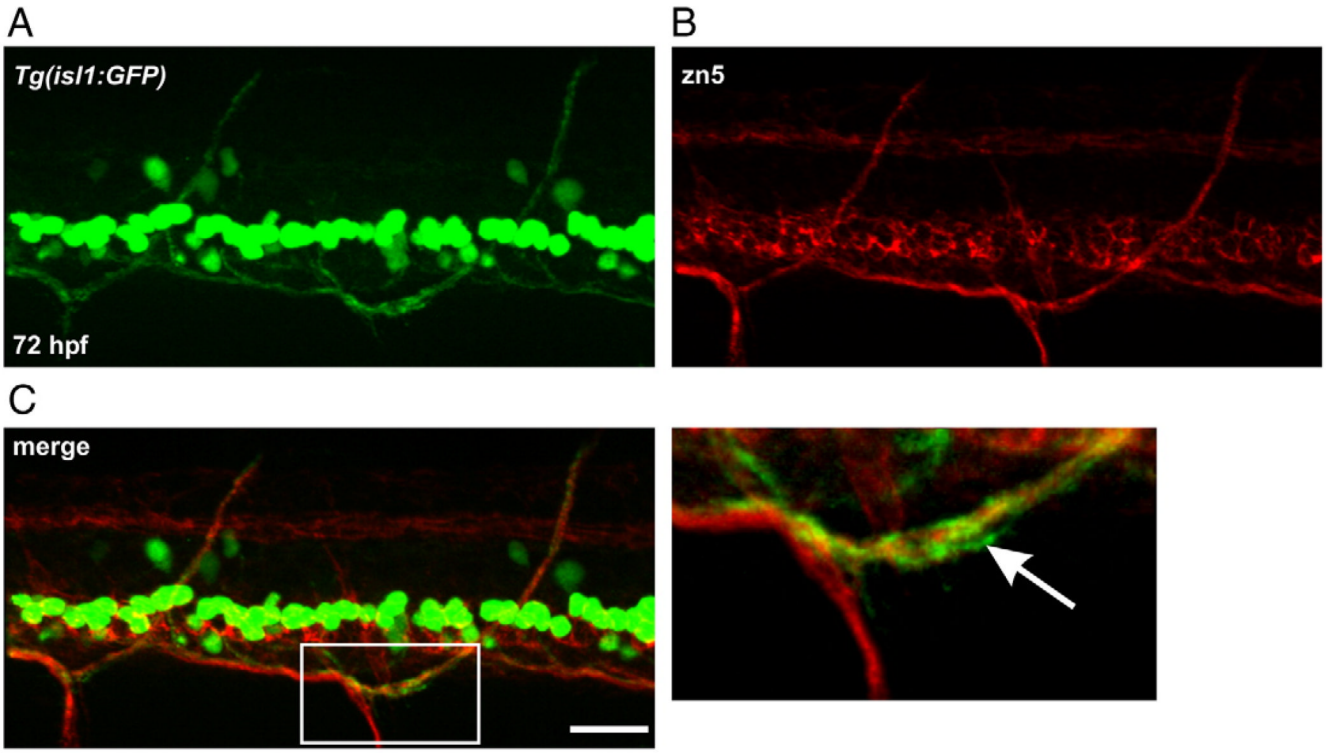

Fig. 7.

zn5 labeling in *Tg(isl1:GFP)* larvae. (A) Photomicrograph of GFP expression in an *isl1* larva. (B) zn5 labeling in the larva shown in A. (C) Merged image reveals that zn5 labels dorsal projecting, GFP-positive secondary motoneuron axons. The white box denotes a region of interest magnified and shown at the right. White arrow points to GFP-positive axon associated with zn5 labeling. Scale bar = 20 μm.

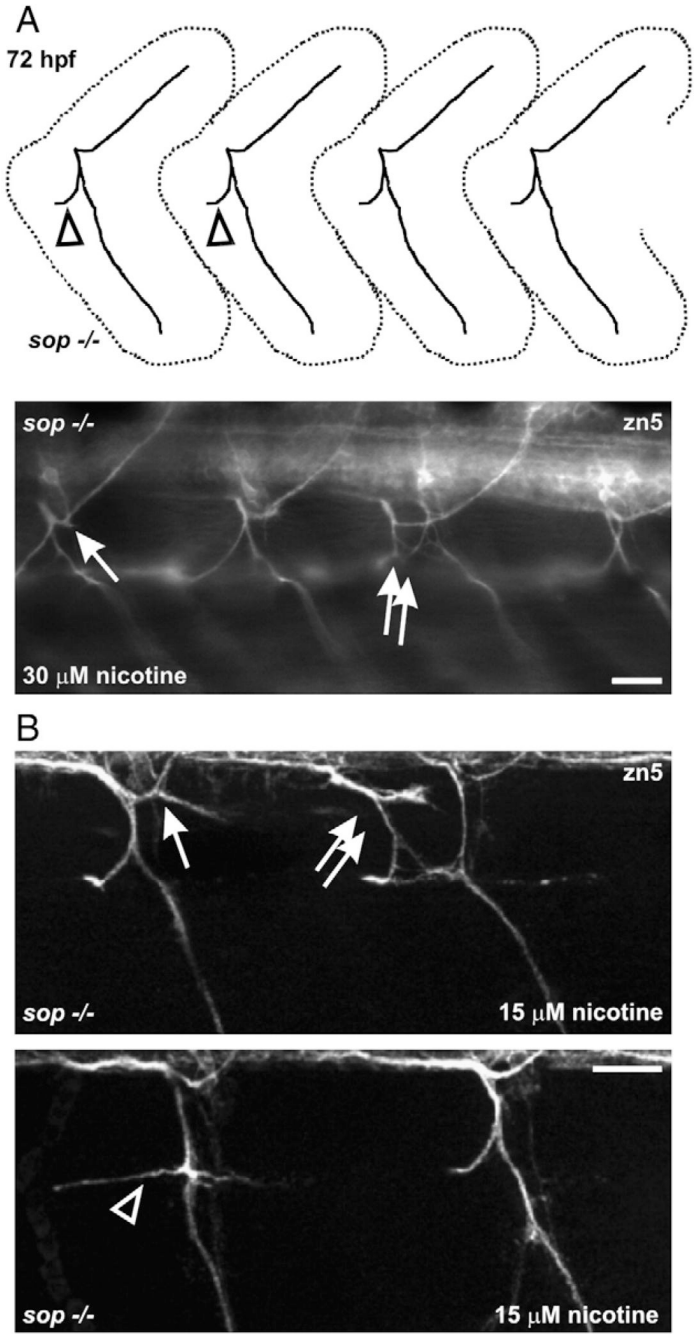

Fig. 8.

Motoneuron axons in nicotine-exposed *sop*$^{-/-}$ larvae. (A) At the top is a cartoon of secondary motoneuron axonal trajectories seen for a 72 hpf *sop*$^{-/-}$ larvae. This pattern is typical of *sop*$^{-/-}$ larvae and wild-type larvae (see Supplement Fig. 1). At the bottom is a photomicrograph of a 72 hpf *sop*$^{-/-}$ larva that was exposed to nicotine. 30 μM nicotine exposure caused pathfinding errors in dorsal projecting axons (arrow); projection is slightly forked. The double white arrows are pointing to duplicated ventral nerves. (B) Photomicrographs of 3D projections obtained from 72 hpf *sop*$^{-/-}$ larvae labeled with zn5 that were exposed to 15 μM nicotine from 22–72 hpf. At the top, nicotine exposure resulted in ectopic branching of a dorsal projecting nerve (white arrow). A duplicated bundle of axons (root) is shown by the double arrows. The

larva shown at the bottom has an abnormal ventral projection (open arrowhead). Compare to axon trajectory shown by open arrowhead in the cartoon shown in A. Errors in secondary motoneuronal axonal pathfinding were detected in 27 of 29 *sop*$^{-/-}$ larvae exposed to nicotine. Scale bars = 20 μm.

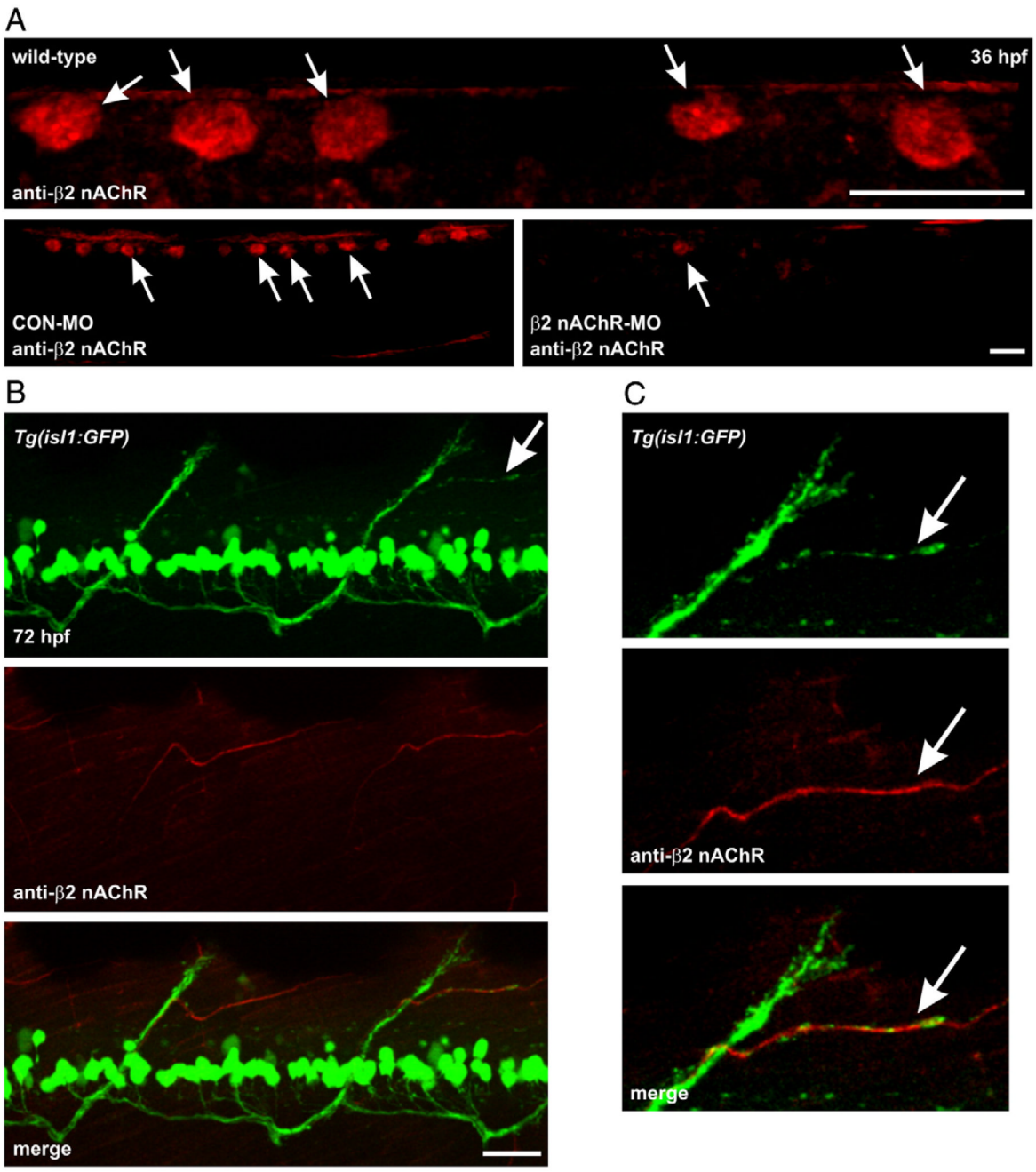

Fig. 9.

β2 nAChR subunits associate with dorsal secondary motoneuron axons in *Tg(isl1:GFP)* zebrafish. (A) Photomicrographs of 36 hpf wild-type embryos labeled with anti-β2 nAChR polyclonal antibody. In the wild-type embryo at the top, the antibody detected RB neurons in dorsal spinal cord. In the embryo at the bottom left which was injected with a control morpholino, the antibody detected RB neurons in dorsal spinal cord. The embryo at the bottom right was injected with a morpholino designed to inhibit β2 nAChR mRNA translation. The morpholino knocked down β2 nAChR expression as revealed by the reduced signal in dorsal spinal cord. (B) At the top is a photomicrograph of GFP expression in an *isl1* larva. White arrow denotes a dorsal projecting nerve that is shown in C. Middle, photomicrograph of β2

nAChR subunit expression in that same larva. Bottom, merged image reveals that β2 nAChR subunits associate with dorsal secondary motoneuron axons. (C) Magnified views of the dorsal projection denoted by the white arrow shown in top panel of B. The β2 nAChR subunit expression is associated with the horizontally projecting GFP-positive axon (white arrow). Scale bars = 20 μm.

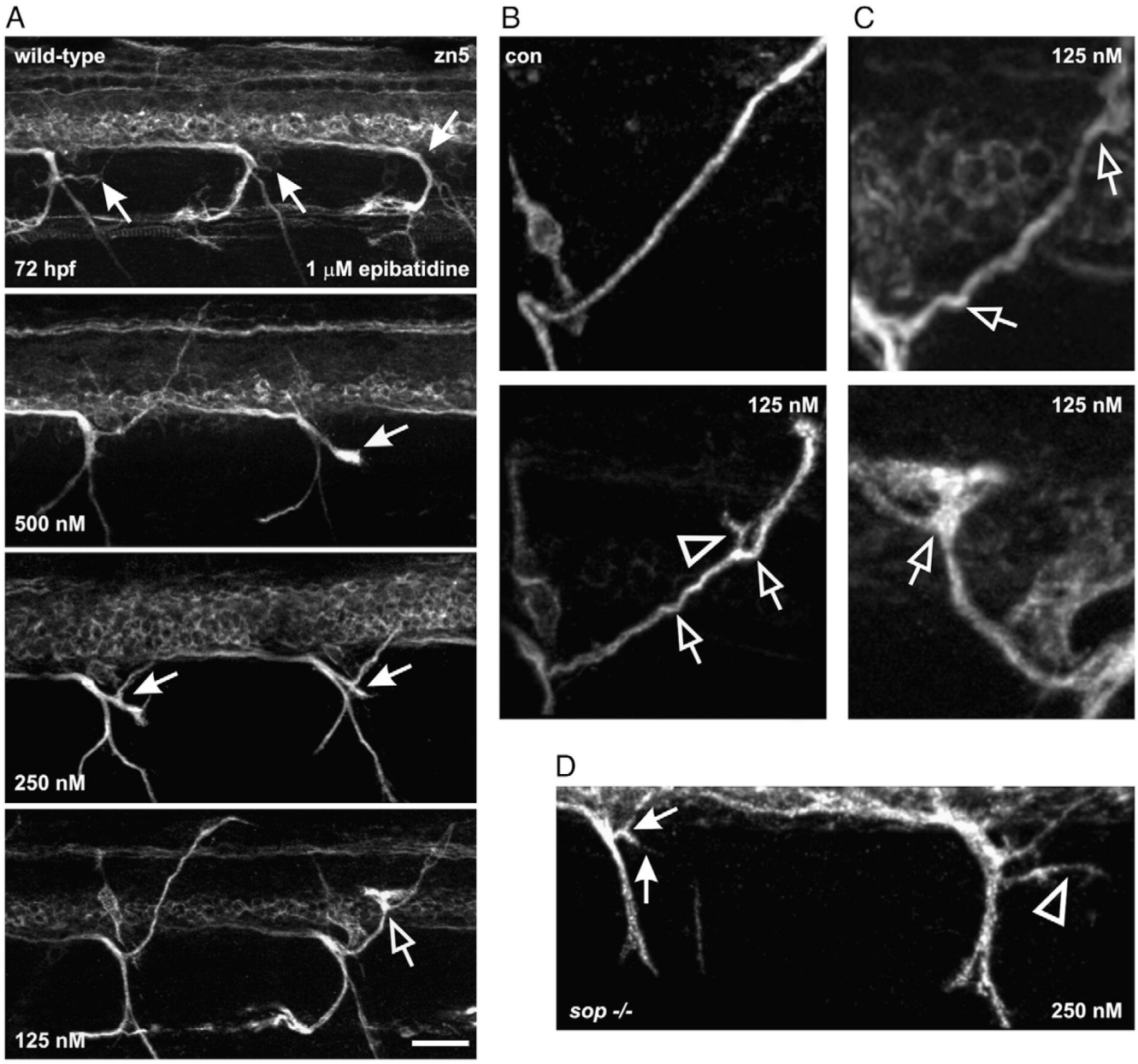

Fig. 10.

Secondary motoneuron axon pathfinding is altered by epibatidine exposure. (A) Photomicrographs of 72 hpf wild-type larvae (n = 42) that were exposed to epibatidine (125 nM, 250 nM, 500 nM and 1 μM) from ~21–72 hpf. By 72 hpf, all dorsal muscle segments should be innervated by a nerve (refer to Fig. 7, zn5 image). In the larva exposed to 1 μM epibatidine, zn5-positive dorsal secondary axons have not projected into the periphery (denoted by white arrows). See panel B (top) for control (con) image showing one dorsal nerve extending well into periphery. In the larva exposed to 500 nM epibatidine, 1 dorsal projection in the field of view extended into the periphery while the other denoted by the white arrow stalled. Axons in larvae exposed to 250 and 125 nM epibatidine still exhibited pathfinding errors. The white arrows in the 250 nM-exposed larva point to nerves that "forked" entering the periphery. The open arrow in the 125 nM image is pointing to a pathfinding error. (B) Magnified views of

dorsal projecting nerves. At the top is an image of a nerve bundle containing zn5-positive axons from a control larva. At the bottom is an image of a nerve bundle from a larva exposed to 125 nM epibatidine. The open arrows point to “kinks” in the nerve. The open arrowhead points to an ectopic branch of the nerve. (C) At the top is an image of a dorsal nerve from a larva exposed to 125 nM epibatidine as it projects to the periphery. At the bottom is a blown up view of the right dorsal axon from the 125 nM-exposed larva in part A. The image has been projected and rotated 180° along its horizontal axis. The nerve made a turn in the wrong direction (open arrow) then corrected itself. (D) Photomicrograph of a 72 hpf $sop^{-/-}$ larva that was exposed to 250 nM epibatidine from 21–72 hpf (n = 12). The dorsal projecting secondary motoneuron nerve denoted by the white arrows forked before it reached the dorsal periphery and projected ventrally. There is also an ectopic zn5-positive motoneuron branch denoted by the arrowhead for the nerve projection at the right. This image is a projection of a z-stack and has been slightly rotated to emphasize the ectopic branch (open arrowhead). Axonal pathfinding errors were detected in all $sop^{-/-}$ larvae exposed to epibatidine. Scale bar = 20 μm.